

1 **Correction of Systematic Model Forcing Bias of CLM using**  
2 **Assimilation of Cosmic-Ray Neutrons and Land Surface**  
3 **Temperature: a study in the Heihe Catchment, China**

4  
5 Xujun Han<sup>1,2,3</sup>, Harrie-Jan Hendricks Franssen<sup>2,3</sup>, Rafael Rosolem<sup>4</sup>, Rui Jin<sup>1,5</sup>, Xin  
6 Li<sup>1,5</sup>, Harry Vereecken<sup>2,3</sup>

- 7  
8 1. Key Laboratory of Remote Sensing of Gansu Province, Cold and Arid Regions  
9 Environmental and Engineering Research Institute, Chinese Academy of Sciences,  
10 Lanzhou 730000, PR China  
11 2. Forschungszentrum Jülich, Agrosphere (IBG 3), Leo-Brandt-Strasse, 52425 Jülich,  
12 Germany  
13 3. Centre for High-Performance Scientific Computing in Terrestrial Systems: HPSC  
14 TerrSys, Geoverbund ABC/J, Leo-Brandt-Strasse, 52425 Jülich, Germany  
15 4. Department of Civil Engineering, University of Bristol, Bristol BS8 1TR, UK  
16 5. CAS Center for Excellence in Tibetan Plateau Earth Sciences, Chinese Academy  
17 of Sciences, Beijing 100101, PR China  
18  
19

20 Corresponding author: Xujun Han, Cold and Arid Regions Environmental and  
21 Engineering Research Institute, Chinese Academy of Sciences, Lanzhou, Gansu  
22 730000, PR China. (hanxj@lzb.ac.cn)  
23

24 **Abstract**

25       The recent development of the non-invasive cosmic-ray soil moisture sensing  
26 technique fills the gap between point scale soil moisture measurements and regional  
27 scale soil moisture measurements by remote sensing. A cosmic-ray probe measures  
28 soil moisture for a footprint with a diameter of ~600 m (at sea level) and with an  
29 effective measurement depth between 12 cm to 76 cm, depending on the soil humidity.  
30 In this study, it was tested whether neutron counts also allow to correct for a  
31 systematic error in the model forcings. Lack of water management data often cause  
32 systematic input errors to land surface models. Here, the assimilation procedure was  
33 tested for an irrigated corn field (Heihe Watershed Allied Telemetry Experimental  
34 Research - HiWATER, 2012) where no irrigation data were available as model input  
35 although for the area a significant amount of water was irrigated. In the study, the  
36 measured cosmic-ray neutron counts and Moderate Resolution Imaging  
37 Spectroradiometer (MODIS) land surface temperature (LST) products were jointly  
38 assimilated into the Community Land Model (CLM) with the Local Ensemble  
39 Transform Kalman Filter. Different data assimilation scenarios were evaluated, with  
40 assimilation of LST and/or cosmic-ray neutron counts, and possibly parameter  
41 estimation of leaf area index (LAI). The results show that the direct assimilation of  
42 cosmic-ray neutron counts can improve the soil moisture and evapotranspiration (ET)  
43 estimation significantly, correcting for lack of information on irrigation amounts. The  
44 joint assimilation of neutron counts and LST could improve further the ET estimation,  
45 but the information content of neutron counts exceeded the one of LST. Additional

46 improvement was achieved by calibrating LAI, which after calibration was also closer  
47 to independent field measurements. It was concluded that assimilation of neutron  
48 counts was useful for ET and soil moisture estimation even if the model has a  
49 systematic bias like neglecting irrigation. However, also the assimilation of LST  
50 helped to correct the systematic model bias introduced by neglecting irrigation and  
51 LST could be used to update soil moisture with state augmentation.

52 **Keywords:** Cosmic-ray neutron counts, Land surface temperature, Evapotranspiration,  
53 Land data assimilation, Parameter estimation

## 54 **1. Introduction**

55 Soil moisture plays a key role for crop and plant growth, water resources  
56 management and land surface-atmosphere interaction. Therefore accurate soil  
57 moisture retrieval is important. Point scale measurements can be obtained by methods  
58 like time domain reflectometry (TDR) (Robinson et al., 2003) and larger scale, coarse  
59 soil moisture information from remote sensing sensors (Entekhabi et al., 2010; Kerr et  
60 al., 2010). Wireless Sensor Networks (WSN) allow characterization of soil moisture at  
61 the catchment scale with many local connected sensors at separated locations (Bogena  
62 et al., 2010). TDR only measures the point scale soil moisture and the maintenance of  
63 WSN is expensive. Recently, neutron count intensity measured by above-ground  
64 cosmic-ray probes was proposed as alternative information source on soil moisture.  
65 Neutron count intensity is measured non-invasively at an intermediate scale between  
66 the point scale and the coarse remote sensing scale (Zreda et al., 2008). A network of  
67 cosmic-ray sensors (CRS) has been set-up over N-America (Zreda et al., 2012).

68 Cosmic rays are composed of primary protons mainly. The fast neutrons  
69 generated by high-energy neutrons colliding with nuclei lead to “evaporation” of fast  
70 neutrons and the generated and moderated neutrons in the ground can diffuse back  
71 into the air where their intensity can be measured by the cosmic-ray soil moisture  
72 probe. Soil moisture affects the rate of moderation of fast neutrons, and controls the  
73 neutron concentration and the emission of neutrons into the air. Dry soils have low  
74 moderating power and are highly emissive; wet soils have high moderating power and  
75 are less emissive. The neutrons are mainly moderated by the hydrogen atoms

76 contained in the soil water and emitted to the atmosphere where the neutrons mix  
77 instantaneously at a scale of hundreds of meters. The measurement area of a  
78 cosmic-ray soil moisture probe represents a circle with a diameter of ~600 m at sea  
79 level (Desilets and Zreda, 2013) and the measurement depth decreases non-linearly  
80 from ~76 cm (dry soils) to ~12 cm (saturated soils) (Zreda et al., 2008). The measured  
81 cosmic-ray neutron counts show an inverse correlation with soil moisture content. The  
82 cosmic-ray neutron intensity could be reduced to 60% of surface cosmic-ray neutron  
83 intensity if the soil moisture was increased from zero to 40% (Zreda et al., 2008). The  
84 soil moisture estimation on the basis of cosmic-ray probe based neutron counts over a  
85 horizontal footprint of hectometers received considerable attention in scientific  
86 literature during the last years (Desilets et al., 2010; Zreda et al., 2008; Zreda et al.,  
87 2012).

88       Hydrogen atoms are present as water in the soil, lattice soil water, below ground  
89 biomass, atmospheric water vapor, snow water, above ground biomass, intercepted  
90 water by vegetation and water on the ground. These additional hydrogen sources  
91 contribute to the measured neutron intensity. The role of these additional hydrogen  
92 sources should be included in the analysis of the cosmic-ray measurements in order to  
93 isolate the main contribution from soil moisture. Formulations for handling water  
94 vapor (Rosolem et al., 2013), for lattice water and organic carbon (Franz et al., 2013)  
95 and for a litter layer present on the soil surface (Bogena et al., 2013) have been  
96 developed.

97       The positive impact of soil moisture data assimilation was shown in several

98 studies. Importantly, surface soil moisture could be used to obtain better  
99 characterization of the root zone soil moisture (Barrett and Renzullo, 2009; Crow et  
100 al., 2008; Das et al., 2008; Draper et al., 2011; Li et al., 2010). It was also shown that  
101 the assimilation of soil moisture observations can be used to correct rainfall errors  
102 (Crow et al., 2011; Yang et al., 2009). Often a systematic bias between measured and  
103 modelled soil moisture content can be found; soil moisture estimation can be  
104 significantly improved using joint state and bias estimation (De Lannoy et al., 2007;  
105 Kumar et al., 2012; Reichle, 2008). Also studies on data assimilation of remotely  
106 sensed land surface temperature products show a positive impact on the estimation of  
107 soil moisture, latent heat flux and sensible heat flux (Ghent et al., 2010; Xu et al.,  
108 2011). Also in these studies it was found that bias, in these cases soil temperature bias,  
109 of land surface models can be removed with land surface temperature assimilation  
110 (Bosilovich et al., 2007; Reichle et al., 2010). Other studies updated both land surface  
111 model states and parameters with soil moisture and land surface temperature data  
112 (Bateni and Entekhabi, 2012; Han et al., 2014a; Montzka et al., 2013; Pauwels et al.,  
113 2009). The assimilation of measured cosmic-ray neutron counts in a land surface  
114 model was successfully tested, but these studies focused on state updating alone  
115 (Rosolem et al., 2014; Shuttleworth et al., 2013). In this paper we focus on the  
116 assimilation of measured cosmic-ray neutron counts for improving soil moisture  
117 content characterization at the field scale. This paper focuses on the case that model  
118 input is biased. Land surface models still are affected by limited knowledge on water  
119 resources management and for regions in China (and elsewhere) typically no

120 information on irrigation amounts is available as irrigation is mainly by the flooding  
121 system. We analyse whether measured neutron counts are able to correct for such  
122 biases. This case is not only relevant for neglecting irrigation in China, but also for  
123 other water resources management issues (e.g., groundwater pumping) which are  
124 neglected in the simulations. Neglecting irrigation in land surface models results in a  
125 large bias in the simulated soil moisture content because of a lack of water input. The  
126 bias in soil moisture content also results in a too small latent heat flux and too high  
127 sensible heat flux. We hypothesize that data assimilation also can play an important  
128 role for removing such biases in data deficient areas. One possible strategy in data  
129 assimilation studies for handling this type of bias, which is not followed in this paper,  
130 is to calibrate the simulation model (e.g., land surface model) prior to data  
131 assimilation to remove biases (Kumar et al., 2012) and use the corrected simulation  
132 model in the context of sequential data assimilation. A different strategy was followed  
133 in this paper and no a priori bias correction was carried out because this type of  
134 problem (neglecting water resources management) does not allow for such an a priori  
135 bias correction. The bias can be attributed to the model structure, model parameters,  
136 atmospheric forcing or observation data, and the bias-aware assimilation requires the  
137 assumption that the bias comes from a particular source. If the source of bias is not  
138 attributed to the right source, model predictions cannot be improved (Dee, 2005).  
139 Therefore bias-blind assimilation was used for safety and the bias estimation was not  
140 handled explicitly. Instead, we investigated whether neutron counts measured by  
141 cosmic-ray probe were able to correct for the bias. Aim is to improve the soil moisture

142 profile estimation in a crop land with seed corn as main crop type.

143 In CLM, land surface fluxes are calculated based on the Monin-Obukhov  
144 similarity theory. The sensible heat flux is formulated as a function of temperature and  
145 LAI, and the latent heat flux is formulated as a function of the temperature and leaf  
146 stomatal resistances. The leaf stomatal resistance is calculated from the Ball-Berry  
147 conductance model (Collatz et al., 1991). The updates of soil temperature and  
148 vegetation temperature are derived based on the solar radiation absorbed by top soil  
149 (or vegetation), longwave radiation absorbed by soil (or vegetation), sensible heat flux  
150 from soil (or vegetation) and latent heat flux from soil (or vegetation). Measured land  
151 surface temperature is composed of the ground temperature and vegetation  
152 temperature. Therefore a difference between measured and calculated land surface  
153 temperature can be adjusted by changing land surface fluxes. As land surface fluxes  
154 are sensitive to soil moisture content, land surface temperature is sensitive to soil  
155 moisture content.

156 Therefore, the land surface temperature (LST) products measured by the  
157 Moderate Resolution Imaging Spectroradiometer (MODIS) Terra (MOD11A1) and  
158 Aqua (MYD11A1) are also assimilated jointly to improve the soil temperature profile  
159 estimation because the evapotranspiration is sensitive to the soil temperature. Two  
160 Terra LST products can be obtained per day at 10:30 am/pm and two Aqua LST  
161 products can be obtained per day at 1:30 am/pm. Soil moisture, land surface  
162 temperature and LAI influence the estimation of latent and sensible heat fluxes  
163 (Ghilain et al., 2012; Jarlan et al., 2008; Schwinger et al., 2010; van den Hurk, 2003;



164 Yang et al., 1999), and therefore this study also focused on the calibration of LAI with  
165 help of the assimilation of land surface temperature. However, there are large  
166 discrepancies between the remotely retrieved LAI and measured values, and the  
167 MODIS LAI product underestimates in situ measured LAI by 44% on average  
168 (<http://landval.gsfc.nasa.gov/>), and therefore the LAI is also calibrated by data  
169 assimilation. In summary, the novel aspects of this work are: 1) investigating whether  
170 data assimilation is able to correct for missing water resources management data  
171 without a priori bias correction; 2) joint assimilation of cosmic-ray neutron counts,  
172 LST and updating of LAI; 3) application of this framework to real-world data in an  
173 irrigated area where detailed verification data were available.

174

## 175 **2. Materials and Methods**

### 176 **2.1 Study Area and Measurement**

177 The Heihe River Basin is the second largest inland river basin of China, and it is  
178 located between  $97.1^{\circ}$  E- $102.0^{\circ}$  E and  $37.7^{\circ}$  N- $42.7^{\circ}$  N and covers an area of  
179 approximately 143,000 km<sup>2</sup> (Li et al., 2013). In 2012, a multi-scale observation  
180 experiment of evapotranspiration with a well-equipped superstation (Daman  
181 superstation) to measure the atmospheric forcings and soil moisture at 2 cm, 4 cm, 10  
182 cm, 20 cm, 40 cm, 80 cm, 120 cm and 160 cm depth (Xu et al., 2013), was carried out  
183 from June to September in the framework of the Heihe Watershed Allied Telemetry  
184 Experimental Research (HiWATER) (Li et al., 2013). SoilNet wireless network nodes  
185 (Bogena et al., 2010) were deployed to measure soil moisture content and soil

186 temperature at four layers (4 cm, 10 cm, 20 cm and 40 cm). One cosmic-ray soil  
187 moisture probe (CRS-1000B) was installed (Han et al., 2014b) with 23 SoilNet nodes  
188 (Jin et al., 2014; Jin et al., 2013) in the footprint (Fig. 1). The main crop type within  
189 the footprint of the cosmic-ray probe is seed corn. The irrigation is applied through  
190 channels using the flooding irrigation method. Exact amounts of applied irrigation are  
191 therefore not available.

192 The measured cosmic-ray neutron count data were processed to remove the  
193 outliers according to the sensor voltage ( $\leq 11.8$  Volt) and relative humidity ( $\geq 80\%$ )  
194 (Zreda et al., 2012). The surface fluxes were measured using the eddy covariance  
195 technique, and data were processed using EdiRe  
196 (<http://www.geos.ed.ac.uk/abs/research/micromet/EdiRe>) software, in which the  
197 anemometer coordinate rotation, signal lag removal, frequency response correction,  
198 density corrections and signal de-spiking were done for the raw data. The energy  
199 balance closure was not considered in this study. The LAI was measured by the  
200 LAI-2000 scanner during the field experiment, there are 17 samples collected in 14  
201 days of 3 months.

202 [\[Insert Figure 1 here\]](#)

203

## 204 **2.2 Land Surface Model and Data**

205 The CLM was used to simulate the spatio-temporal distribution of soil moisture,  
206 soil temperature, land surface temperature, vegetation temperature, sensible heat flux,  
207 latent heat flux and soil heat flux of the study area. The coupled water and energy

208 balance are modeled in CLM, and the land surface heterogeneity is represented by  
209 patched plant functional types and soil texture (Oleson et al., 2013).

210 The soil properties used in CLM were from the soil database of China with 1 km  
211 spatial resolution (Shangguan et al., 2013). The MODIS 500 m resolution plant  
212 functional type product (MCD12Q1) (Sun et al., 2008) which was resampled by  
213 nearest neighbor interpolation to 1 km resolution and MODIS LAI product  
214 (MCD15A3) with 1 km spatial resolution (Han et al., 2012) were used as input. Due  
215 to a lack of measurement data, two atmospheric forcing data sets were used: the  
216 Global Land Data Assimilation System reanalysis data (Rodell et al., 2004) was  
217 interpolated using the National Centers for Environmental Prediction (NCEP) bilinear  
218 interpolation library iplib in spatial and temporal dimensions and used in the CLM for  
219 the spin-up period ([http://www.nco.ncep.noaa.gov/pmb/docs/libs/ipilib/ncep\\_ipilib.sht-](http://www.nco.ncep.noaa.gov/pmb/docs/libs/ipilib/ncep_ipilib.sht-ml)  
220 [ml](http://www.nco.ncep.noaa.gov/pmb/docs/libs/ipilib/ncep_ipilib.sht-ml)). For the three months data assimilation period, hourly forcing data (incident  
221 longwave radiation, incident solar radiation, precipitation, air pressure, specific  
222 humidity, air temperature and wind speed) from the Daman superstation of HiWATER  
223 were available and used.

224

### 225 **2.3 Cosmic-Ray Forward Model**

226 In this study, the new developed COsmic-ray Soil Moisture Interaction Code  
227 (COSMIC) model (Shuttleworth et al., 2013) was used as the cosmic-ray forward  
228 model to simulate the cosmic-ray neutron count rate using the soil moisture profile as  
229 input. The effective measurement depth of the cosmic-ray soil moisture probe ranges

230 from 12 cm (wet soils) to 76 cm (dry soils) (Zreda et al., 2008), within which 86% of  
 231 the above-ground measured neutrons originate. COSMIC also calculates the effective  
 232 sensor depth based on the cosmic-ray neutron intensity and the soil moisture profile  
 233 values (Franz et al., 2012; Shuttleworth et al., 2013).

234 COSMIC makes several assumptions to calculate the number of fast neutrons  
 235 reaching the cosmic-ray soil moisture probe ( $N_{COSMOS}$ ) at a near-surface measurement  
 236 location. The soil layer with a depth of 3 meters for the complete soil profile, was  
 237 discretized into 300 layers for the integration of Eq. 2 in COSMIC. The number of  
 238 fast neutrons reaching the cosmic-ray probe  $N_{COSMOS}$  is formulated as (Shuttleworth  
 239 et al., 2013):

$$240 \quad N_{COSMOS} = N \int_0^{\infty} \left\{ A(z) [\alpha \rho_s(z) + \rho_w(z)] \exp \left( - \left[ \frac{m_s(z)}{L_1} + \frac{m_w(z)}{L_2} \right] \right) \right\} dz \quad (1)$$

$$241 \quad A(z) = \left( \frac{2}{\pi} \right)^{\pi/2} \int_0^{\pi/2} \exp \left( \frac{-1}{\cos(\theta)} \left[ \frac{m_s(z)}{L_3} + \frac{m_w(z)}{L_4} \right] \right) d\theta \quad (2)$$

$$242 \quad \alpha = 0.405 - 0.102 \rho_s \quad (3)$$

$$243 \quad L_3 = -31.76 + 99.38 \rho_s \quad (4)$$

244 where  $N$  is the high energy neutron intensity (counts/hour),  $z$  denotes the soil  
 245 layer depth (m),  $\rho_s$  the dry soil bulk density ( $\text{g/cm}^3$ ),  $\rho_w$  the total water density,  
 246 including the lattice water ( $\text{g/cm}^3$ ) and  $\alpha$  denotes the ratio of fast neutron creation  
 247 factor.  $L_1$  is the high energy soil attenuation length with value of  $162.0 \text{ g/cm}^2$  and  
 248  $L_2$  the high energy water attenuation length of  $129.1 \text{ g/cm}^2$ . In equation (2)  $\theta$  is the  
 249 angle between the vertical below the detector and the line between the detector and  
 250 each point in the plane,  $m_s(z)$  and  $m_w(z)$  are the integrated mass per unit area of

251 dry soil and water ( $\text{g}/\text{cm}^2$ ), respectively.  $L_3$  denotes the fast neutron soil attenuation  
252 length ( $\text{g}/\text{cm}^2$ ) and  $L_4$  stands for the fast neutron water attenuation length with value  
253 of  $3.16 \text{ g}/\text{cm}^2$ .

254 The cosmic-ray neutron intensity reaching the land surface is influenced by air  
255 pressure, atmospheric water vapor content and incoming neutron flux. In order to  
256 isolate the contribution of soil moisture content to the measured neutron density, it is  
257 important to take these effects into account and the calibrated neutron count intensity  
258 can be derived as follows:

$$259 \quad N_{Corr} = N_{Obs} f_p f_{wv} f_i \quad (5)$$

260 where  $N_{Corr}$  represents corrected neutron counts and  $N_{Obs}$  the measured  
261 neutron counts.  $f_p$  is the correction factor for air pressure,  $f_{wv}$  the correction  
262 factor for atmospheric water vapor and  $f_i$  the correction factor for incoming neutron  
263 flux.

264 The correction factor for air pressure  $f_p$  can be calculated as (Zreda et al.,  
265 2012):

$$266 \quad f_p = \exp\left(\frac{P - P_0}{L}\right) \quad (6)$$

267 where  $P$  (mbar) is the local air pressure,  $P_0$  (mbar) the average air pressure  
268 during the measurement period and  $L$  ( $\text{g}/\text{cm}^2$ ) is the mass attenuation length for  
269 high-energy neutrons; the default value of  $128 \text{ g}/\text{cm}^2$  was used in this study (Zreda et  
270 al., 2012).

271 The correction factor  $f_{wv}$  for atmospheric water vapor is calculated as (Rosolem  
272 et al., 2013):

273 
$$f_{wv} = 1 + 0.0054(\rho_{v0} - \rho_{v0}^{ref}) \quad (7)$$

274 where  $\rho_{v0}$  (k/gm<sup>3</sup>) is the absolute humidity at the measurement time and  $\rho_{v0}^{ref}$   
275 (kg/m<sup>3</sup>) is the average absolute humidity during the measurement period.

276 Fluctuations in the incoming neutron flux should be removed because the  
277 cosmic-ray probe is designed to measure the neutron flux based on the incoming  
278 background neutron flux. The correcting factor  $f_i$  for the incoming neutron flux is  
279 calculated as:

280 
$$f_i = \frac{N_m}{N_{avg}} \quad (8)$$

281 where  $N_m$  is the measured incoming neutron flux and  $N_{avg}$  is the average  
282 incoming neutron flux during the measurement period. The measured data at the  
283 Jungfrauoch station in Switzerland at 3560 m (<http://cosray.unibe.ch/>) was used to  
284 calculate  $N_m$  and  $N_{avg}$ . The temporal (secular or diurnal) variations caused by the  
285 sunspot cycle could be removed after this correction (Zreda et al., 2012).

286 In this study, the soil moisture for the CRS footprint scale was calculated from the  
287 arithmetic mean of the 23 SoilNet soil moisture observations. The calibration of the  
288 high energy neutron intensity parameter  $N$  in equation (1) was done using the  
289 measured cosmic-ray neutron counts rate and averaged soil moisture content at the  
290 CRS footprint scale. Because lattice water was unknown for this site, a value of 3%  
291 was assumed in this study (Franz et al., 2012). Hourly soil moisture measurements for  
292 a period of 2.5 months were used for COSMIC calibration. Inside the cosmic-ray  
293 probe footprint, the amount of applied irrigation was spatially variable due to the  
294 different management practice of each farmer. The gradient search algorithm

295 L-BFGS-B (Zhu et al., 1997) was used to minimize the root mean square error of the  
296 differences between simulated cosmic-ray neutron counts (using measured soil  
297 moisture by SoilNet as input to COSMIC) and the measured neutron counts  $N_{Corr}$ .  
298 The optimized parameter value of  $N$  was 615.96 counts/hour in this case.

299 The simulated soil moisture content for 10 CLM soil layers (3.8 m depth) was  
300 used as input to COSMIC in order to simulate the corresponding neutron count  
301 intensity and compare it with the measured neutron count intensity. It should be  
302 mentioned that it is unlikely that anything beyond 1 m depth will substantially impact  
303 the results because the effective measurement depth of the cosmic-ray probe is  
304 between 12 and 76 cm. The COSMIC model assumes a more detailed soil profile.  
305 COSMIC interpolates the soil moisture information from the ten CLM soil layers to  
306 information for 300 soil layers of depth 1cm. The contribution of each soil layer to the  
307 measured neutron flux will change temporally depending on the soil moisture  
308 condition. Therefore the effective measurement depth of the cosmic ray probe will  
309 also change temporally. COSMIC calculates the vertically weighted soil moisture  
310 content based on the vertical distribution of soil moisture content.

311

## 312 **2.4 Two Source Formulation - TSF**

313 The land surface temperature products of MODIS are composed of a ground  
314 temperature and vegetation temperature component, which are however unknown.  
315 CLM models the ground temperature and vegetation temperature separately, but does  
316 not model the composed land surface temperature as seen by MODIS. The

317 corresponding land surface temperature of CLM should therefore be modelled for  
 318 data assimilation purposes. The two source formulation (Kustas and Anderson, 2009)  
 319 was used in this study to calculate the land surface temperature from the MODIS view  
 320 angle using ground temperature and vegetation temperature simulated by CLM:

$$321 \quad T_s = [F_c(\Phi)T_c^4 + (1 - F_c(\Phi)T_g^4)]^{1/4} \quad (9)$$

322 where  $T_s$  (K) is the composed surface temperature as seen by the MODIS sensor,  
 323  $F_c(\Phi)$  is the fraction vegetation cover observed from the sensor view angle  $\Phi$   
 324 (radians),  $T_c$  (K) is the vegetation temperature and  $T_g$  (K) is the ground temperature.  
 325 (Kustas and Anderson, 2009):

$$326 \quad F_c(\Phi) = 1 - \exp\left(\frac{-0.5\Omega(\Phi)LAI}{\cos\Phi}\right) \quad (10)$$

327 where  $LAI$  is the leaf area index,  $\Omega(\Phi)$  is a clumping index to represent the  
 328 nonrandom leaf area distributions of farmland or other heterogeneous land surfaces  
 329 (Anderson et al., 2005), and is defined as:

$$330 \quad \Omega(\Phi) = \frac{0.49\Omega_{\max}}{0.49 + (\Omega_{\max} - 0.49)\exp(k\theta^{3.34})} \quad (11)$$

$$331 \quad \Omega_{\max} = 0.49 + 0.51(\sin\Phi)^{0.05} \quad (12)$$

$$332 \quad k = -\{0.3 + [0.833(\sin\Phi)^{0.1}]^{14}\} \quad (13)$$

333

## 334 **2.5 Assimilation Approach**

335 The Local Ensemble Transform Kalman Filter (LETKF) was used as the  
 336 assimilation algorithm, which is one of the square root variants of the ensemble  
 337 Kalman filter (Evensen, 2003; Hunt et al., 2007; Miyoshi and Yamane, 2007). The  
 338 model uncertainties are represented using the ensemble simulation of model states and



339 LETKF derives the background error covariance using the model state ensemble  
340 members. LETKF uses the non-perturbed observations to update all the ensemble  
341 members of model states at each assimilation step.

342 In this study,  $x_1^b, \dots, x_N^b$  denote the model state ensemble members;  $\bar{x}^b$  is the  
343 ensemble mean of  $x_1^b, \dots, x_N^b$ ;  $N$  is the ensemble size;  $y_1^b, \dots, y_N^b$  denote the mapped  
344 model state ensemble members;  $\bar{y}^b$  is the ensemble mean of  $y_1^b, \dots, y_N^b$ ;  $H$  is the  
345 observation operator (COSMIC for soil moisture or the two source function for land  
346 surface temperature). The analysis step of LETKF can be summarized as follows:

347 Prepare the model state vector  $X^b$ :

$$348 \quad X^b = [x_1^b - \bar{x}^b, \dots, x_N^b - \bar{x}^b] \quad (14)$$

349 where  $\bar{x}^b$  is composed of one vertically weighted soil moisture content and soil  
350 moisture content for 10 CLM-layers, resulting in a state dimension equal to 11 if only  
351 the neutron count observation was assimilated; and  $\bar{x}^b$  is composed of surface  
352 temperature, ground temperature, vegetation temperature and soil temperature for 15  
353 CLM-layers if only the land surface temperature observations were assimilated  
354 without soil moisture update, giving a state dimension of 18. The water and energy  
355 balance are coupled, and in CLM the energy balance is firstly solved, then the derived  
356 surface fluxes are used for updating soil moisture content. The cross correlation  
357 between the soil temperature and soil moisture can be calculated using the ensemble  
358 prediction in LETKF, and this makes the updating of soil moisture by assimilating  
359 land surface temperature possible. We also used the land surface temperature to  
360 update the soil moisture profile, in this case the soil moisture vector was augmented to

361 the LETKF state vector of land surface temperature assimilation, resulting in a state  
362 dimension of 28.

363 Construct the mapped model state vector  $Y^b$  after transformation of observation  
364 operator:

$$365 \quad y_i^b = H(x_i^b) \quad (15)$$

$$366 \quad Y^b = [y_1^b - \bar{y}^b, \dots, y_N^b - \bar{y}^b] \quad (16)$$

367 The following analysis is looped for each model grid cell to calculate the update  
368 of model state ensemble members:

369 Calculate analysis error covariance matrix  $P^a$ :

$$370 \quad P^a = [(N - 1)I + Y^{bT}R^{-1}Y^b] \quad (17)$$

371 where  $I$  is the identity matrix.

372 The perturbations in ensemble space are calculated as:

$$373 \quad W^a = [(N - 1)P^a]^{1/2} \quad (18)$$

374 Calculate the analysis mean  $\bar{w}^a$  in ensemble space and add to each column of  
375  $W^a$  to get the analysis ensemble in ensemble space:

$$376 \quad \bar{w}^a = P^a Y^{bT} R^{-1} (y^o - \bar{y}^b) \quad (19)$$

377 Calculate the new analysis:

$$378 \quad X^a = X^b [\bar{w}^a + W^a] + \bar{x}^b \quad (20)$$

379 where  $R$  is the observation error covariance matrix,  $y^o$  is the observation vector  
380 and  $X^a$  contains the updated model ensemble members.

381 The LETKF method can also be extended to do parameter estimation using a state  
382 augmentation approach (Bateni and Entekhabi, 2012; Li and Ren, 2011; Moradkhani

383 et al., 2005; Nie et al., 2011). Alternative strategies for parameter estimation are a dual  
384 approach (Moradkhani et al., 2005) with separate updating of states and parameters.  
385 Vrugt et al. (2005) also proposed a dual approach with parameter updating in an outer  
386 optimization loop using a Markov Chain Monte Carlo method, and state updating in  
387 an inner loop. The a priori calibration of model parameters is also an option (Kumar et  
388 al., 2012). With the augmentation approach, the state vector of LETKF can be  
389 augmented by the parameter vector including soil properties (sand fraction, clay  
390 fraction and organic matter density) and vegetation parameters (LAI, etc.). In a  
391 preliminary sensitivity study it was found that for this site simulation results were  
392 more sensitive to the LAI than to soil properties. Soil texture is also quite well known  
393 for this site from measurements. Therefore in this study, only the LAI was in some of  
394 the simulation scenarios calibrated. In the different scenarios of land surface  
395 temperature assimilation, the LETKF state vector was also augmented to include LAI  
396 as calibration target. As a consequence, the augmented state vector contains surface  
397 temperature, ground temperature, and vegetation temperature, 15 layers of soil  
398 temperature and LAI, making up a state dimension equal to 19 for the scenarios of  
399 land surface temperature assimilation without soil moisture update; for the scenarios  
400 of land surface temperature with soil moisture update, the state dimension is 29. The  
401 10 layers of soil moisture and 15 layers of soil temperature are the standard CLM  
402 layout for both soil moisture and soil temperature. The hydrology calculations are  
403 done over the top 10 layers, and the bottom 5 layers are specified as bedrock. The  
404 lower 5 layers are hydrologically inactive layers. Temperature calculations are done

405 over all layers (Oleson et al., 2013).

406

### 407 **3. Experiment Setup**

408 First the 50 ensemble members of CLM with perturbed soil properties and  
409 atmospheric forcing data were driven from the 1<sup>st</sup> of Jan. 2012 to the 31<sup>st</sup> of May 2012  
410 to do the CLM spin-up; second an additional assimilation period of cosmic-ray  
411 neutron counts was done from the 1<sup>st</sup> of Jun. 2012 to the 30<sup>th</sup> Aug. 2012 to reduce the  
412 spin-up error. The final CLM states on the 30<sup>th</sup> of Aug. 2012 were used as the initial  
413 states for the 1<sup>st</sup> of Jun. 2012 for the data assimilation scenarios. Perturbed soil  
414 properties were generated by adding a spatially uniform perturbation sampled from a  
415 uniform distribution between -10% and 10% to the values extracted from the Soil  
416 Database of China for Land Surface Modeling (1 km spatial resolution). The LAI was  
417 perturbed with multiplicative uniform distributed random noise in the range of  
418 [0.8~1.2]. The perturbations added to the model forcings show correlations in space  
419 and time. The spatial correlation was induced by a Fast Fourier Transform and the  
420 temporal correlation by a first-order auto-regressive model (Han et al., 2013; Kumar  
421 et al., 2009; Reichle et al., 2010). The statistics on the perturbation of the forcing data  
422 are summarized in Table 1. The values of standard deviations and temporal  
423 correlations in Table 1 were chosen based on previous catchment scale and regional  
424 scale data assimilation studies (De Lannoy et al., 2012; Kumar et al., 2012; Reichle et  
425 al., 2010).

426 [\[Insert Table 1 here\]](#)

427 The cosmic-ray neutron intensity was assimilated every 3 days at 12Z from the 1<sup>st</sup>  
428 of June 2012 onwards. We found that the differences between daily assimilation and 3  
429 days assimilation were small, therefore only the results of 3 days assimilation are  
430 shown. The measured neutron count intensity showed large temporal fluctuations in  
431 time and these fluctuations were not corresponding to the temporal variations of soil  
432 moisture. Therefore the measured neutron count intensity was smoothed with the  
433 Savitzky–Golay filter using a moving average window of size 31 hours and a  
434 polynomial of order 4 (Savitzky and Golay, 1964). The originally measured neutron  
435 counts and smoothed neutron counts are plotted in Fig. 2. The assimilation frequency  
436 of MODIS LST products of MOD11A1 and MYD11A1 was up to 4 times (maximum)  
437 per day depending on the data availability. There are 230 observation data (including  
438 cosmic-ray probe neutron counts, MODIS LST, MOD11A1 and MYD11A1 LST) in  
439 the whole assimilation window. The variance of the instantaneous measured neutron  
440 intensity is equal to the measured neutron count intensity (Zreda et al., 2012) and  
441 smaller for temporal averaging for daily or sub-daily applications. The instantaneous  
442 neutron intensity was assimilated in this study. The variance of MODIS LST was  
443 assumed to be 1 K (Wan and Li, 2008).

444 The 4 days MODIS LAI product was aggregated and used as the CLM LAI  
445 parameter. Because the LAI from MODIS is usually lower than the true value  
446 (compared with the field measured LAI in the HiWATER experiment) and because the  
447 surface flux and surface temperature are sensitive to the LAI, two additional scenarios  
448 were investigated where LAI was calibrated to study the impact of LAI estimation on

449 surface flux estimation within the data assimilation framework.

450 The following assimilation scenarios were compared: (1) CLM: open loop  
451 simulation without assimilation; (2) Only\_CRS: only the measured neutron counts  
452 were assimilated; (3) Only\_LST: only the MODIS LST products were assimilated.  
453 The quality control flags of LST products were used to select the data with good  
454 quality for assimilation; (4) CRS\_LST: the measured neutron counts and MODIS LST  
455 products were assimilated jointly. In the above scenarios, the neutron count data was  
456 used to update the soil moisture and the LST data were used to update the ground  
457 temperature, vegetation temperature and soil temperature. (5) LST\_Feedback: We also  
458 evaluated the scenario of assimilating the LST measurements to update the soil  
459 moisture profile. (6) CRS\_LST\_Par\_LAI: the LAI was included as variable to be  
460 calibrated, otherwise the scenario was the same as CRS\_LST. (7)  
461 LST\_Feedback\_Par\_LAI: the LAI was included as variable to be calibrated,  
462 otherwise the scenario was the same as LST\_Feedback. (8) CRS\_LST\_True\_LAI: the  
463 in situ measured LAI during the HiWATER experiment was used in the model  
464 simulation.

465 [\[Insert Figure 2 here\]](#)

466

#### 467 **4. Results and Discussion**

468 In order to evaluate the assimilation results for the different scenarios outlined in  
469 section 3, the Root Mean Square Error (RMSE) was used:

$$470 \quad \text{RMSE} = \sqrt{\frac{\sum_{n=i}^N (\text{Estimated} - \text{Measured})^2}{N}} \quad (21)$$

471 where “*Estimated*” is the ensemble mean without assimilation or the ensemble  
472 mean after assimilation, “*Measured*” is measured soil moisture content evaluated at  
473 the SoilNet nodes (or latent heat flux, sensible heat flux or soil heat flux).  $N$  is the  
474 number of time steps. For the soil moisture analysis in this study,  $N$  is equal to 2184.  
475 The smaller the RMSE value is, the closer assimilation results are to measured values,  
476 which is in general considered to be desirable.

477 The temporal evolution of soil moisture content at 10, 20, 50 and 80 cm depth for  
478 different scenarios is plotted in Fig. 3 and Fig. 4. The RMSE values for different  
479 scenarios are summarized in Table 2. Assimilating the land surface temperature could  
480 improve the soil moisture profile estimation in the scenario of  
481 LST\_Feedback\_Par\_LAI; the soil moisture results are better than the open loop run at  
482 all depths. With the assimilation of CRS neutron counts, the soil moisture RMSE  
483 values at 10 cm and 20 cm depth (scenarios CRS\_LST\_Par\_LAI and  
484 CRS\_LST\_True\_LAI) decreased significantly. The RMSE values for the scenarios  
485 Only\_CRS and CRS\_LST (not shown) are similar to CRS\_LST\_Par\_LAI, which  
486 indicates that the main improvement for the soil moisture profile characterization is  
487 achieved by neutron count assimilation; and land surface temperature assimilation and  
488 LAI estimation play a minor role. Without assimilation of cosmic-ray probe neutron  
489 counts, the soil moisture simulation cannot be improved (scenario Only\_LST).  
490 However, the scenarios of LST\_Feedback and LST\_Feedback\_Par\_LAI improve the  
491 soil moisture profile characterization, which shows that explicitly using LST to update  
492 soil moisture content in the data assimilation routine gives better results than using

493 LST only to update soil moisture by the model equations. Results of LST\_Feedback  
494 and LST\_Feedback\_Par\_LAI are similar; therefore only results for  
495 LST\_Feedback\_Par\_LAI are shown in Fig. 3 and Fig. 4. This implies that the  
496 improved soil moisture characterization due to LAI calibration is low. The results for  
497 the cosmic-ray probe neutron count assimilation proved that the cosmic-ray probe  
498 sensor can be used to improve the soil moisture profile estimation at the footprint  
499 scale.

500 [\[Insert Figure 3 here\]](#)

501 [\[Insert Figure 4 here\]](#)

502 [\[Insert Table 2 here\]](#)

503 Fig. 5 depicts the scatter plots of measured ET versus modelled ET for different  
504 scenarios, and the accumulated ET for all scenarios are summarized in the lower-right  
505 corner of Fig. 5. The EC measured evapotranspiration (ET) is 384.7 mm for the  
506 assimilation period, without energy balance closure correction. The true  
507 evapotranspiration is therefore likely larger, but not much larger as the energy balance  
508 gap was limited (3.7%). The CLM estimated ET, without data assimilation, using only  
509 precipitation as input is 223.7 mm and is much smaller than the measured value as  
510 applied irrigation is not considered in the model. This open loop simulated value  
511 would imply water stress and a limitation of canopy transpiration and soil evaporation  
512 due to low soil moisture content. Assimilation of land surface temperature only  
513 (Only\_LST) hardly affected the estimated ET and was not able to correct for the  
514 artificial water stress condition. However, if land surface temperature was used to



515 update soil moisture directly, taking into account correlations between the two states  
516 in the data assimilation routine, the ET estimates improved to 336.8 mm and 354.8  
517 mm for the scenarios of LST\_Feedback and LST\_Feedback\_Par\_LAI respectively.  
518 The assimilation of land surface temperature of MODIS with soil moisture update  
519 results in significant improvements of ET.

520 The different neutron count assimilation scenarios also resulted in significantly  
521 improved estimates of ET. Univariate assimilation of cosmic-ray neutron data  
522 (Only\_CRS) resulted in 301.9 mm ET. This shows that the impact of neutron count  
523 assimilation to correct evapotranspiration estimates is slightly smaller than the impact  
524 of land surface temperature with soil moisture update. Joint assimilation of land  
525 surface temperature data and cosmic-ray neutron data (CRS\_LST) gave a slightly  
526 larger ET of 310.6 mm than Only\_CRS. Scenarios of CRS\_LST\_Par\_LAI and  
527 CRS\_LST\_True\_LAI gave the best ET estimates (360.5 mm and 349.3 mm). This  
528 shows that correcting the biased LAI-estimates from MODIS by in situ data or  
529 calibration helped to improve model estimates.

530 [\[Insert Figure 5 here\]](#)

531 The RMSE values of latent heat flux, sensible heat flux and soil heat flux for all  
532 scenarios are summarized in Fig. 6. It is obvious that the RMSE values are very large  
533 for both the latent heat flux ( $123.9 \text{ W/m}^2$ ) and sensible heat flux ( $80.5 \text{ W/m}^2$ ) for the  
534 open loop run and all other scenarios where the soil moisture was not updated. If the  
535 land surface temperature was assimilated to update the soil moisture, the latent heat  
536 flux RMSE decreased to  $60.5 \text{ W/m}^2$  (LST\_Feedback) and  $62.5 \text{ W/m}^2$

537 (LST\_Feedback\_Par\_LAI). The scenario where soil moisture and LAI are jointly  
538 updated (LST\_Feedback\_Par\_LAI) gave worse results than the scenario of  
539 LST\_Feedback. Again, the assimilation of neutron counts also resulted in a strong  
540 RMSE reduction for the latent heat flux ( $76.5 \text{ W/m}^2$  for Only\_CRS). If in addition  
541 land surface temperature was assimilated and LAI optimized, the RMSE value of  
542 latent heat flux further decreased to  $56.1 \text{ W/m}^2$  ( $70.7 \text{ W/m}^2$  without LAI optimization).  
543 If the field measured LAI was used instead in the assimilation (CRS\_LST\_True\_LAI),  
544 the RMSE was  $61.0 \text{ W/m}^2$ . These results are in correspondence with the ones  
545 discussed before for soil moisture characterization. Evidently, the combined  
546 assimilation of cosmic-ray probe neutron counts and land surface temperature, and  
547 calibration of LAI (or use of field measured LAI as model input) shows the strongest  
548 improvement for the estimation of land surface fluxes. The soil heat flux did not show  
549 a clear improvement related to assimilation and showed only some improvement in  
550 case LAI was calibrated. For the scenario of land surface temperature assimilation  
551 without soil moisture update (Only\_LST), estimates of latent and sensible heat flux  
552 are not improved. It means that under water stress condition, the improved  
553 characterization of land surface temperature (and soil temperature) does not contribute  
554 to a better estimation of land surface fluxes.

555 [\[Insert Figure 6 here\]](#)

556 The updated LAI for scenarios of LST\_Feedback\_Par\_LAI and  
557 CRS\_LST\_Par\_LAI is shown in Fig. 7. The MODIS LAI product was used as input  
558 for CLM and time series are plotted as blue line in Fig. 7 (Background). The LAI was

559 also measured in the HiWATER experiment, and the measured values are shown as  
560 green star (Observation). Ens\_Mean represents the mean LAI of all ensemble  
561 members (Ensembles). It is obvious that MODIS underestimates the LAI compared  
562 with the observations. With the assimilation of land surface temperature, the LAI  
563 could be updated and be closer to the observations, but there is still a significant  
564 discrepancy between the measured LAI and the updated one. The LAI values for the  
565 scenario with LAI calibration (CRS\_LST\_Par\_LAI) are close to the measured LAI  
566 values (CRS\_LST\_True\_LAI), which is an encouraging result. The calibrated LAI  
567 shows some unrealistic increases and decreases during the assimilation period, which  
568 is inherent to the data assimilation approach. A smoothed representation of the LAI  
569 might provide a more realistic picture.

570 [\[Insert Figure 7 here\]](#)

571 This study illustrates that for an irrigated farmland, the measured cosmic-ray  
572 probe neutron counts can be used to improve the soil moisture profile estimation  
573 significantly. Without irrigation data, CLM underestimated soil moisture content. The  
574 cosmic-ray neutron count data assimilation can be used as an alternative way to  
575 retrieve the soil moisture content profile in CLM. The improved soil moisture  
576 simulation was helpful for the characterization of the land surface fluxes. The  
577 univariate assimilation of land surface temperature without soil moisture update is not  
578 helpful for the estimation of land surface fluxes and even worsened the sensible heat  
579 flux characterization (Fig. 6). However, in a multivariate data assimilation framework  
580 where land surface temperature was assimilated together with measured cosmic-ray

581 probe neutron counts, the land surface temperature assimilation contributed  
582 significantly to an improved ET estimation. The simulated canopy transpiration in  
583 CLM was in general too low, even when the water stress condition was corrected by  
584 assimilating neutron counts, which was related to small values of the LAI. The  
585 additional estimation of LAI through the land surface temperature assimilation  
586 resulted in an increase of the LAI yielding an increase of estimated ET.

587 In general, land surface models need to be calibrated before use in land data  
588 assimilation, especially if there is an apparent large bias in the model simulation (Dee,  
589 2005). The simulation of soil moisture and surface fluxes was biased in our study,  
590 mainly due to the lack of irrigation water as input. This bias cannot be corrected a  
591 priori without exact irrigation data, which are not available in the field. The data  
592 assimilation was proven to be an efficient way to remove the model bias in this case.  
593 We also calculated the equivalent water depth to analyze the equivalent irrigated  
594 water after each step of soil moisture update. For the scenarios of CRS\_LST\_Par\_LAI  
595 and CRS\_LST\_True\_LAI, the equivalent irrigation in three months was 693.6 mm  
596 and 607.6 mm, respectively. Because the irrigation method is flood irrigation, it is not  
597 easy to evaluate the true irrigation applied in the field. From the results we see  
598 however that the applied irrigation (in the model) is much larger than actual ET  
599 (~600-700mm vs ~400mm). This could indicate that the amount of applied irrigation  
600 in the model is too large, but irrigation by flooding is also inefficient and results in  
601 excess runoff and infiltration to the groundwater, because it cannot be controlled as  
602 well as sprinkler irrigation or drip irrigation. Therefore, the calculated amount of

603 irrigation could be realistic, but might also be too large if soil properties are erroneous  
604 in the model.

605 The soil moisture content measured by the cosmic-ray probe represents the depth  
606 between 12 cm (very humid) and 76 cm (extremely dry case) depending on the  
607 amount of soil water (soil moisture content and lattice water). Therefore the effective  
608 sensor depth of the cosmic-ray probe will change over time. In order to model the  
609 variable sensor depth and the relationship between the soil moisture content and  
610 neutron counts, the new developed COSMIC model was used as the observation  
611 operator in this study. Additionally the influences of air pressure, atmospheric vapor  
612 pressure and incoming neutron counts were removed from the original measured  
613 neutron counts. Because there is still some water in the crop which also affects the  
614 cosmic-ray probe sensor, the COSMIC observation operator could be improved to  
615 include vegetation effects. Several default parameters proposed by (Shuttleworth et al.,  
616 2013) were used in the COSMIC model and these parameters probably need further  
617 calibration following the development of the COSMIC model.

618 The spatial distribution of soil moisture for the study area was very  
619 heterogeneous due to the small farmland patches and different irrigation periods for  
620 the different farmlands. Therefore the soil moisture content inferred by SoilNet may  
621 not represent the true soil moisture content of the cosmic-ray probe footprint, which is  
622 a further limitation of this study. Although the Cosmic-ray Soil Moisture Observing  
623 System (COSMOS) has been designed as a continental scale network by installing  
624 500 COSMOS probes across the USA (Zreda et al., 2012), there are still some

625 disadvantages of COSMOS compared with remote sensing. COSMOS is also  
626 expensive for extensive deployment to measure the continental/regional scale soil  
627 moisture.

## 628 **5. Summary and Conclusions**

629 In this paper, we studied the univariate assimilation of MODIS land surface  
630 temperature products, the univariate assimilation of measured neutron counts by the  
631 cosmic-ray probe, the bivariate assimilation of land surface temperature and neutron  
632 count data, and the additional calibration of LAI for an irrigated farmland at the Heihe  
633 catchment in China, where data on the amount of applied irrigation were lacking. The  
634 most important objective of this study was to test whether data assimilation is able to  
635 correct for the absence of information on water resources management as model input,  
636 a situation commonly encountered in large scale land surface modelling. For the  
637 specific case of lacking irrigation data, no prior bias correction is possible. The bias  
638 blind assimilation without explicit bias estimation was used. We focused on the model  
639 bias introduced by the forcing data and the LAI, and neglected the other sources of  
640 bias. In case LAI was calibrated, this was done at each data assimilation step of land  
641 surface temperature. The data assimilation experiments were carried out with the  
642 CLM and the data assimilation algorithm used was the LETKF. A likely further model  
643 bias, besides missing information on irrigation, is the underestimation of LAI by  
644 MODIS, which was used to force the model.

645 The results show that the direct assimilation of measured cosmic-ray neutron  
646 counts improves the estimation of soil moisture significantly, whereas univariate

647 assimilation of land surface temperature without soil moisture update does not  
648 improve soil moisture estimation. However, if the land surface temperature was  
649 assimilated to update the soil moisture profile directly with help of the state  
650 augmentation method, the evapotranspiration and soil moisture could be improved  
651 significantly. This result suggests that the land surface temperature remote sensing  
652 products are needed to correct the characterization of the soil moisture profile and the  
653 evapotranspiration. The improved soil moisture estimation after the assimilation of  
654 neutron counts resulted in a better ET estimation during the irrigation season,  
655 correcting the too low ET of the open loop simulation. The joint assimilation of  
656 neutron counts and MODIS land surface temperature improved the ET estimation  
657 further compared to neutron count assimilation only. The best ET estimation was  
658 obtained for the joint assimilation of cosmic-ray neutron counts, MODIS land surface  
659 temperature including calibration of the LAI (or if field measured LAI was used as  
660 input). This shows that bias due to neglected information on water resources  
661 management can be corrected by data assimilation if a combination of soil moisture  
662 and land surface temperature data is available.

663 We can conclude that data assimilation of neutron counts and land surface  
664 temperature is useful for ET and soil moisture estimation of an irrigated farmland,  
665 even if irrigation data are not available and excluded from model input. The land  
666 surface temperature measurements are an alternative data source to improve the soil  
667 moisture and land surface fluxes estimation under water stress conditions. This shows  
668 the potential of data assimilation to correct also a systematic model bias. LAI

669 optimization further improves simulation results, which is also likely related to a  
670 systematic underestimation of LAI by the MODIS remote sensing product. The results  
671 of using the calibrated LAI are comparable to the results of using field measured LAI  
672 as model input.

673

## 674 **Acknowledgements**

675 This work is supported by the NSFC (National Science Foundation of China)  
676 project (grant number: 41271357, 91125001), the Knowledge Innovation Program of  
677 the Chinese Academy of Sciences (grant number: KZCX2-EW-312) and the  
678 Transregional Collaborative Research Centre 32, financed by the German Science  
679 foundation. Jungfraujoch neutron monitor data were kindly provided by the  
680 Cosmic-ray Group, Physikalisches Institut, University of Bern, Switzerland. We  
681 acknowledge computing resources and time on the Supercomputing Center of Cold  
682 and Arid Region Environment and Engineering Research Institute of Chinese  
683 Academy of Sciences.

684



685 **List of Tables**

686 Table 1 Summary of perturbation parameters for atmospheric forcing data.

687

688 Table 2 Root Mean Square Error (RMSE) of soil moisture profile of open loop run  
689 (CLM), feedback assimilation of land surface temperature including LAI calibration  
690 (LST\_Feedback\_Par\_LAI), bivariate assimilation of neutron counts and land surface  
691 temperature including LAI calibration (CRS\_LST\_Par\_LAI) and bivariate  
692 assimilation of neutron counts and land surface temperature (CRS\_LST\_True\_LAI).

693

694

Table 1 Summary of perturbation parameters for atmospheric forcing data

<b>Variables</b>	<b>Noise</b>	<b>Standard deviation</b>	<b>Time Correlation scale</b>	<b>Spatial Correlation Scale</b>	<b>Cross correlation</b>
Precipitation	Multiplicative	0.5	24 h	5 km	[ 1.0,-0.8, 0.5, 0.0,
Shortwave radiation	Multiplicative	0.3	24 h	5 km	-0.8, 1.0,-0.5, 0.4,
Longwave radiation	Additive	20 W/m <sup>2</sup>	24 h	5 km	0.5, -0.5, 1.0, 0.4,
Air temperature	Additive	1 K	24 h	5 km	0.0, 0.4, 0.4, 1.0]

696

697

698 Table 2 Root Mean Square Error (RMSE) of soil moisture profile of open loop run  
 699 (CLM), feedback assimilation of land surface temperature including LAI calibration  
 700 (LST\_Feedback\_Par\_LAI), bivariate assimilation of neutron counts and land surface  
 701 temperature including LAI calibration (CRS\_LST\_Par\_LAI) and bivariate  
 702 assimilation of neutron counts and land surface temperature using ground-based  
 703 measured LAI as input (CRS\_LST\_True\_LAI).

Soil Layer Depth	RMSE (m <sup>3</sup> /m <sup>3</sup> )			
	Open Loop (CLM)	LST_Feedback _Par_LAI	CRS_LST _Par_LAI	CRS_LST _True_LAI
10 cm	0.202	0.137	0.085	0.086
20 cm	0.167	0.106	0.047	0.048
50 cm	0.193	0.112	0.112	0.119
80 cm	0.188	0.124	0.136	0.146

704

705

706 **List of Figures**

707 Figure 1. Map of the cosmic-ray probe and SoilNet Nodes in the footprint of the CRS  
708 probe positioned at the Heihe river catchment

709

710 Figure 2. Measured and temporally smoothed CRS neutron counts

711

712 Figure 3. Soil moisture at 10 cm (upper) and 20 cm (lower) depth as obtained from an  
713 open loop run (CLM), local sensors (Obs), and different simulation scenarios. For a  
714 description of the scenarios see section 3 of the paper. The CRS neutron counts were  
715 assimilated from the 1st of June

716

717 Figure 4. Same as figure 3 but for 50 cm (upper) and 80 cm (lower).

718

719 Figure 5. Evapotranspiration estimated according to different scenarios for the period  
720 June-August 2012. For a full description see Fig. 3.

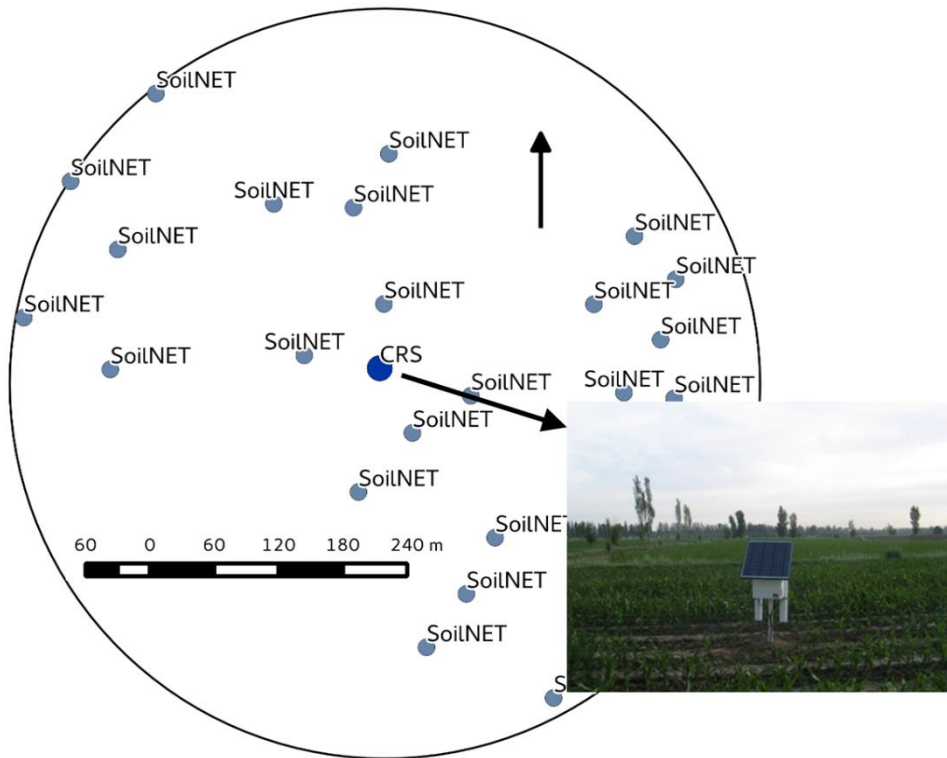
721

722 Figure 6. RMSE values of latent heat flux, sensible heat flux and soil heat flux for the  
723 period June-August 2012. For a description of the scenarios see section 3 of the paper.

724

725 Figure 7. LAI evolution for the period June-August 2012. Displayed are the measured  
726 LAI (Observation), default values (Background), mean of ensemble members  
727 (Ens\_Mean) and ensemble members (Ensembles) for scenarios of  
728 LST\_Feedback\_Par\_LAI (upper) and CRS\_LST\_Par\_LAI (lower)

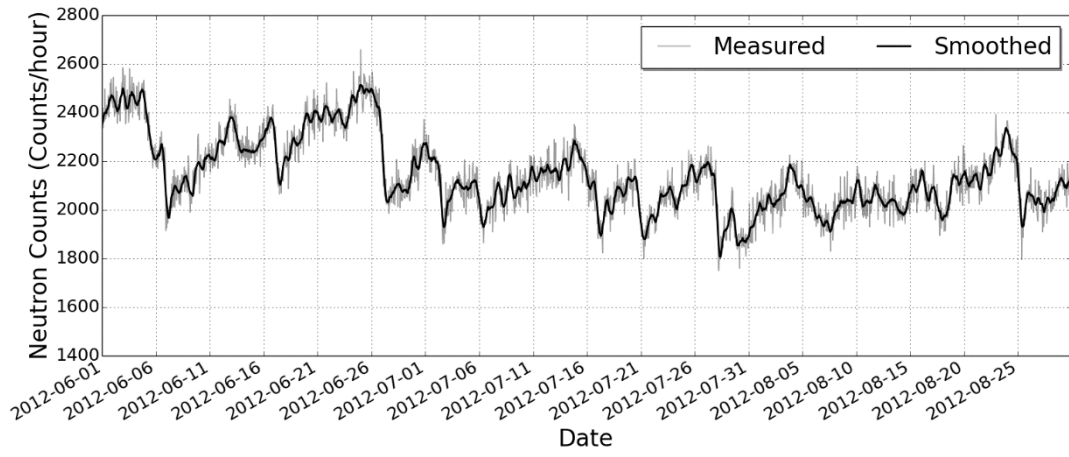
729



730

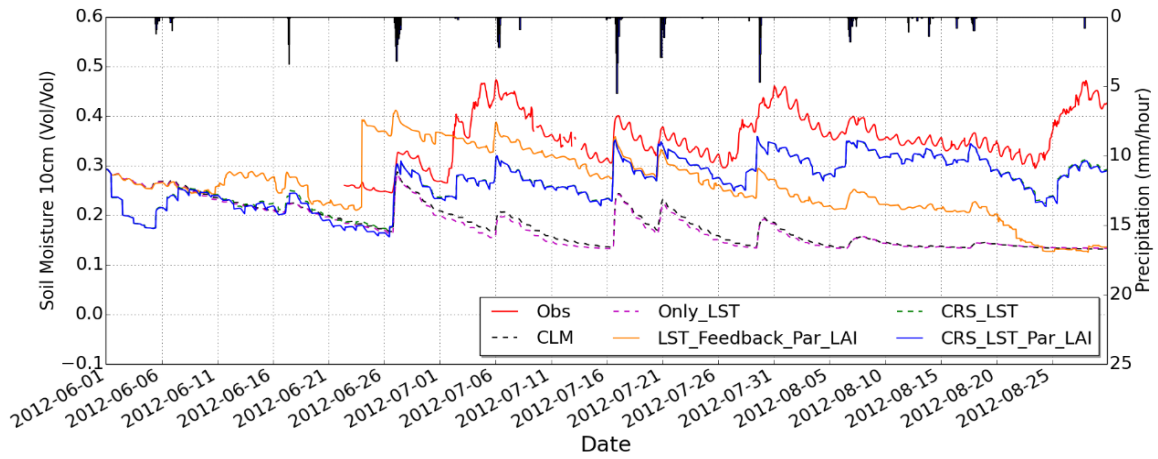
731 Figure 1. Map of the cosmic-ray probe and SoilNet Nodes in the footprint of the CRS  
 732 probe positioned at the Heihe river catchment

733

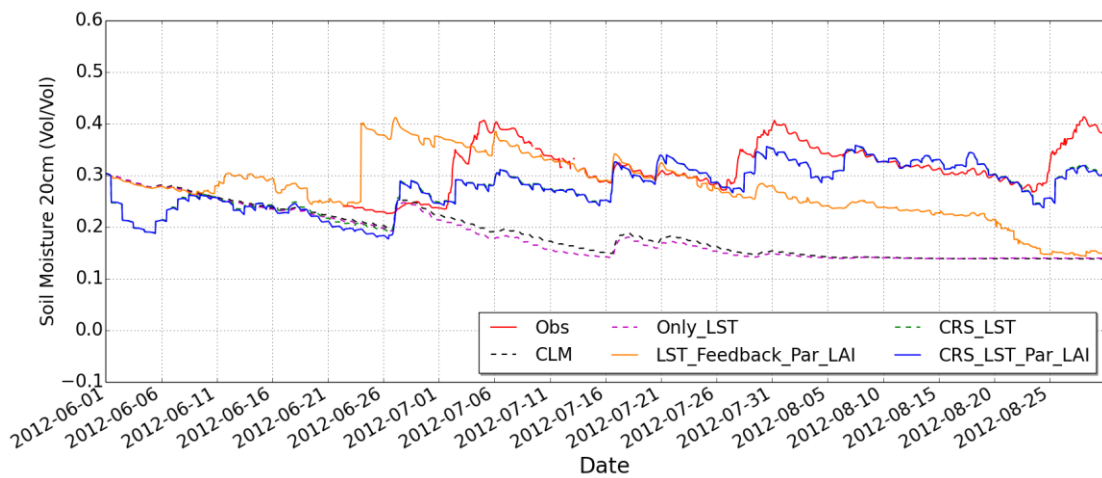


734  
735  
736

Figure 2. Measured and temporally smoothed CRS neutron counts

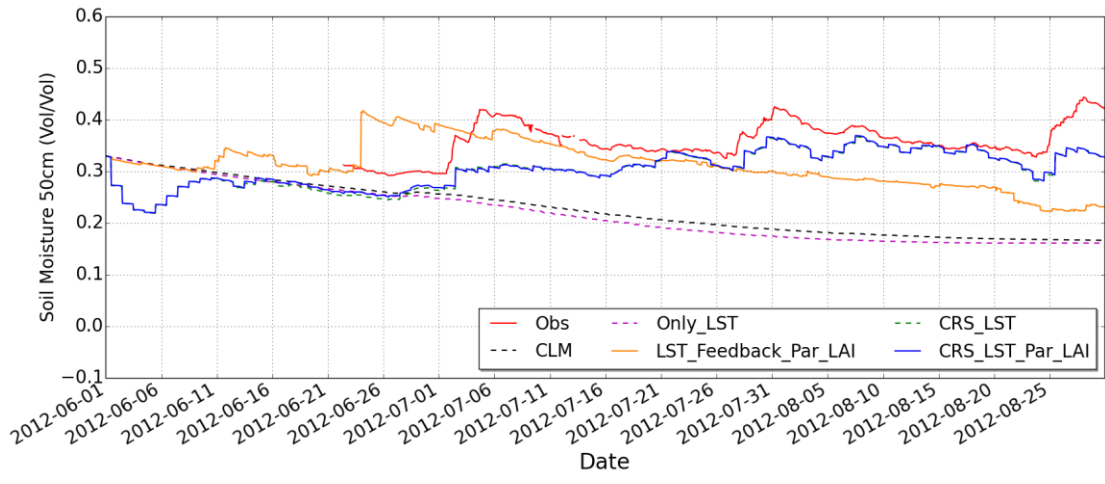


737

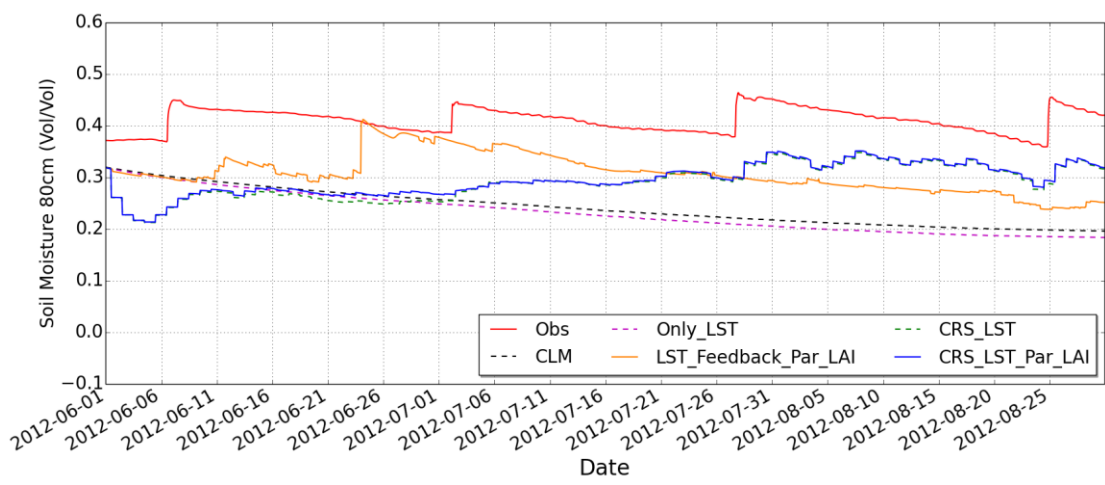


738

739 Figure 3. Soil moisture at 10 cm (upper) and 20 cm (lower) depth as obtained from an  
 740 open loop run (CLM), local sensors (Obs), and different simulation scenarios. For a  
 741 description of the scenarios see section 3 of the paper. The CRS neutron counts were  
 742 assimilated from the 1<sup>st</sup> of June onwards.  
 743



744



745

746

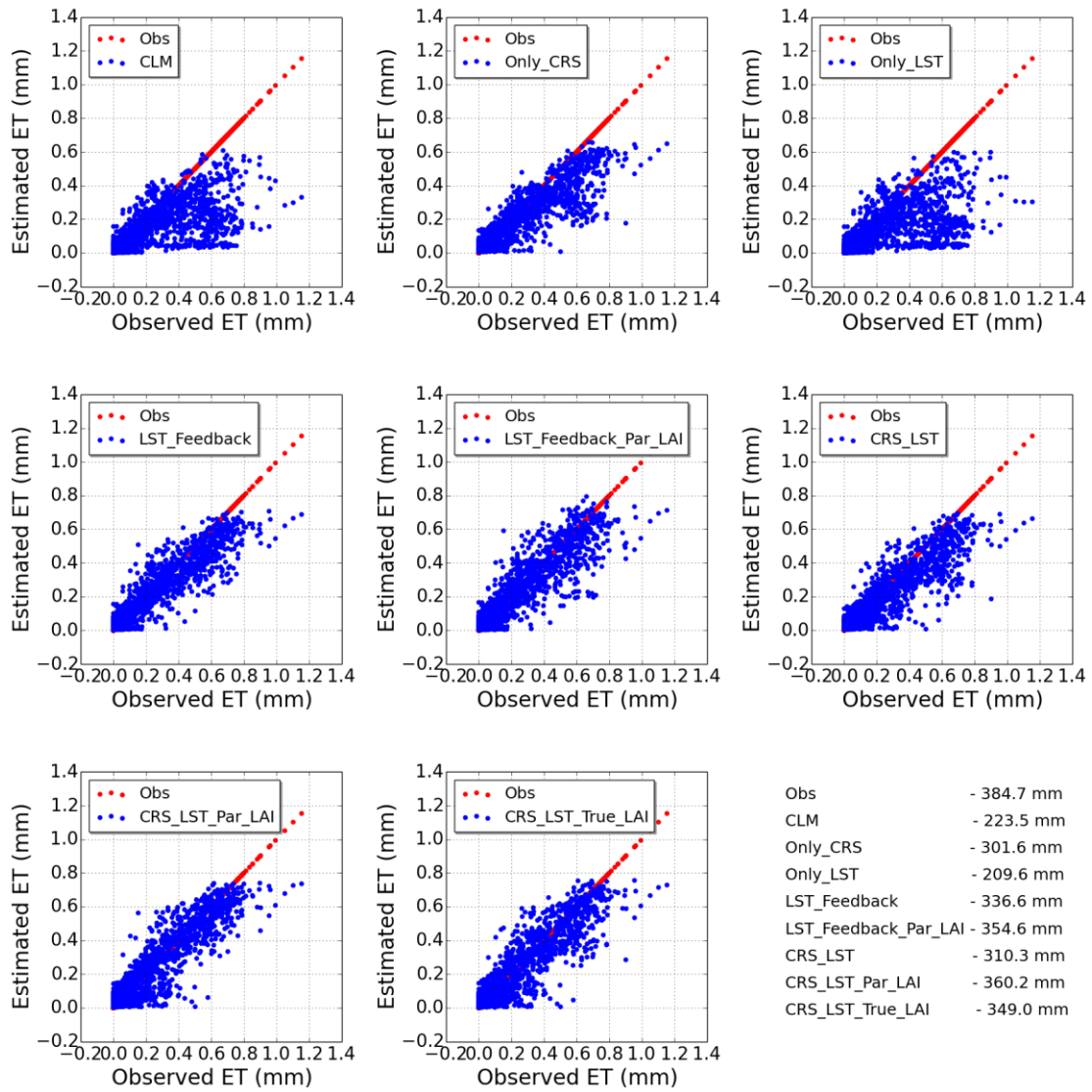
747

748

749

Figure 4. Same as figure 3 but for 50 cm (upper) and 80 cm (lower).





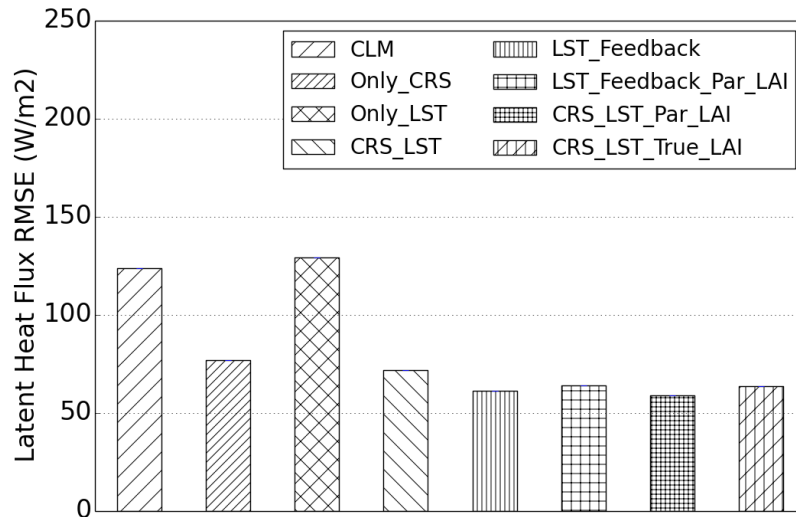
750

751 Figure 5. Evapotranspiration estimated according to different scenarios for the period

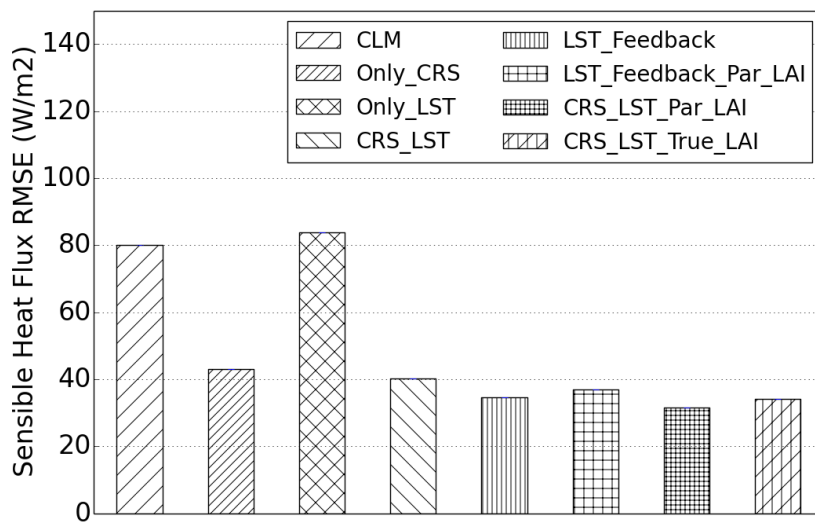
752

June-August 2012. For a full description see Fig. 3.

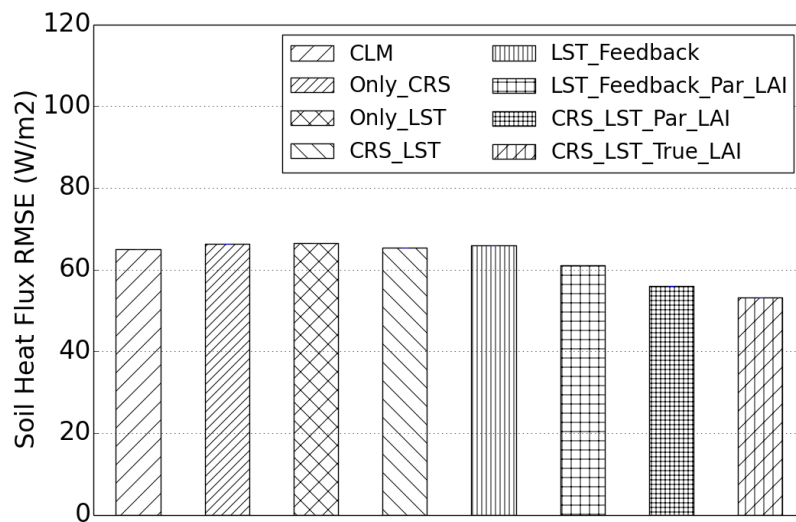
753



754



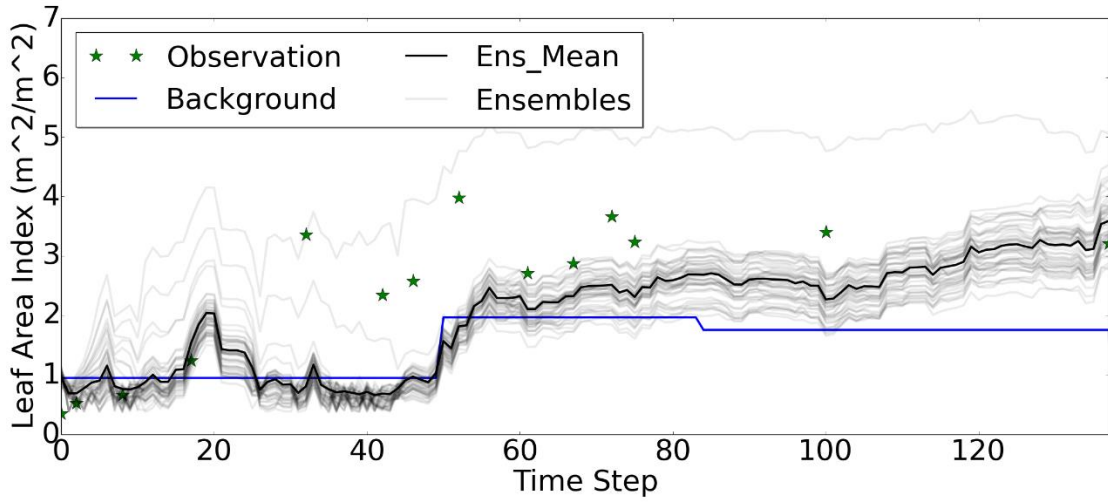
755



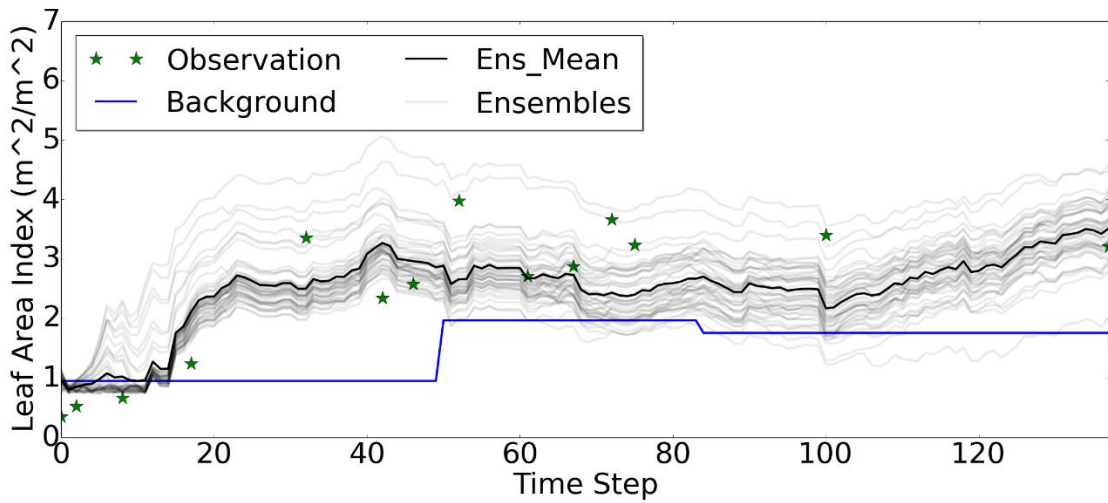
756

757 Figure 6. RMSE values of latent heat flux, sensible heat flux and soil heat flux for the  
 758 period June-August 2012. For a description of the scenarios see section 3 of the paper.  
 759

759



760



761

762 Figure 7. LAI evolution for the period June-August 2012. Displayed are the measured  
 763 LAI (Observation), default values (Background), mean of ensemble members  
 764 (Ens\_Mean) and ensemble members (Ensembles) for scenarios of  
 765 LST\_Feedback\_Par\_LAI (upper) and CRS\_LST\_Par\_LAI (lower)

766

767

768 **References:**

- 769 Anderson, M. C., Norman, J. M., Kustas, W. P., Li, F., Prueger, J. H., and Mecikalski, J. R.: Effects of  
770 Vegetation Clumping on Two-Source Model Estimates of Surface Energy Fluxes from an Agricultural  
771 Landscape during SMACEX, *J Hydrometeorol*, 6, 892-909, 2005.
- 772 Barrett, D. J. and Renzullo, L. J.: On the Efficacy of Combining Thermal and Microwave Satellite Data as  
773 Observational Constraints for Root-Zone Soil Moisture Estimation C-7972-2009, *J Hydrometeorol*, 10,  
774 1109-1127, 2009.
- 775 Bateni, S. M. and Entekhabi, D.: Surface heat flux estimation with the ensemble Kalman smoother:  
776 Joint estimation of state and parameters, *Water Resour Res*, 48, 2012.
- 777 Bogena, H. R., Herbst, M., Huisman, J. A., Rosenbaum, U., Weuthen, A., and Vereecken, H.: Potential of  
778 Wireless Sensor Networks for Measuring Soil Water Content Variability, *Vadose Zone J*, 9, 1002-1013,  
779 2010.
- 780 Bogena, H. R., Huisman, J. A., Baatz, R., Hendricks Franssen, H. J., and Vereecken, H.: Accuracy of the  
781 cosmic-ray soil water content probe in humid forest ecosystems: The worst case scenario, *Water*  
782 *Resour Res*, 49, 5778-5791, 2013.
- 783 Bosilovich, M. G., Radakovich, J. D., da Silva, A., Todling, R., and Verter, F.: Skin temperature analysis  
784 and bias correction in a coupled land-atmosphere data assimilation system, *J Meteorol Soc Jpn*, 85A,  
785 205-228, 2007.
- 786 Collatz, G. J., Ball, J. T., Grivet, C., and Berry, J. A.: Physiological and Environmental-Regulation of  
787 Stomatal Conductance, Photosynthesis and Transpiration - a Model That Includes a Laminar  
788 Boundary-Layer, *Agr Forest Meteorol*, 54, 107-136, 1991.
- 789 Crow, W. T., Kustas, W. P., and Prueger, J. H.: Monitoring root-zone soil moisture through the  
790 assimilation of a thermal remote sensing-based soil moisture proxy into a water balance model,  
791 *Remote Sens Environ*, 112, 1268-1281, 2008.
- 792 Crow, W. T., van den Berg, M. J., Huffman, G. J., and Pellarin, T.: Correcting rainfall using satellite-based  
793 surface soil moisture retrievals: The Soil Moisture Analysis Rainfall Tool (SMART), *Water Resour Res*, 47,  
794 2011.
- 795 Das, N. N., Mohanty, B. P., Cosh, M. H., and Jackson, T. J.: Modeling and assimilation of root zone soil  
796 moisture using remote sensing observations in Walnut Gulch Watershed during SMEX04, *Remote Sens*  
797 *Environ*, 112, 415-429, 2008.
- 798 De Lannoy, G. J. M., Houser, P. R., Pauwels, V. R. N., and Verhoest, N. E. C.: State and bias estimation  
799 for soil moisture profiles by an ensemble Kalman filter: Effect of assimilation depth and frequency,  
800 *Water Resour Res*, 43, n/a-n/a, 2007.
- 801 De Lannoy, G. J. M., Reichle, R. H., Arsenault, K. R., Houser, P. R., Kumar, S., Verhoest, N. E. C., and  
802 Pauwels, V. R. N.: Multiscale assimilation of Advanced Microwave Scanning Radiometer-EOS snow  
803 water equivalent and Moderate Resolution Imaging Spectroradiometer snow cover fraction  
804 observations in northern Colorado, *Water Resour Res*, 48, 2012.
- 805 Dee, D. P.: Bias and data assimilation, *Q J Roy Meteor Soc*, 131, 3323-3343, 2005.
- 806 Desilets, D. and Zreda, M.: Footprint diameter for a cosmic-ray soil moisture probe: Theory and Monte  
807 Carlo simulations, *Water Resour Res*, 49, 3566-3575, 2013.
- 808 Desilets, D., Zreda, M., and Ferré, T. P. A.: Nature's neutron probe: Land surface hydrology at an elusive  
809 scale with cosmic rays, *Water Resour. Res.*, 46, W11505, 2010.
- 810 Draper, C. S., Mahfouf, J. F., and Walker, J. P.: Root zone soil moisture from the assimilation of  
811 screen-level variables and remotely sensed soil moisture, *J Geophys Res-Atmos*, 116, 2011.

812 Entekhabi, D., Njoku, E. G., O'Neill, P. E., Kellogg, K. H., Crow, W. T., Edelstein, W. N., Entin, J. K.,  
813 Goodman, S. D., Jackson, T. J., Johnson, J., Kimball, J., Piepmeier, J. R., Koster, R. D., Martin, N.,  
814 McDonald, K. C., Moghaddam, M., Moran, S., Reichle, R., Shi, J. C., Spencer, M. W., Thurman, S. W.,  
815 Tsang, L., and Van Zyl, J.: The Soil Moisture Active Passive (SMAP) Mission, *P IEEE*, 98, 704-716, 2010.  
816 Evensen, G.: The ensemble Kalman filter: Theoretical formulation and practical implementation,  
817 *Ocean Dynam*, 53, 343-367, 2003.  
818 Franz, T. E., Zreda, M., Ferre, T. P. A., Rosolem, R., Zweck, C., Stillman, S., Zeng, X., and Shuttleworth, W.  
819 J.: Measurement depth of the cosmic ray soil moisture probe affected by hydrogen from various  
820 sources, *Water Resour Res*, 48, 2012.  
821 Franz, T. E., Zreda, M., Rosolem, R., and Ferre, T. P. A.: A universal calibration function for  
822 determination of soil moisture with cosmic-ray neutrons, *Hydrology and Earth System Sciences*, 17,  
823 453-460, 2013.  
824 Ghent, D., Kaduk, J., Remedios, J., Ardo, J., and Balzter, H.: Assimilation of land surface temperature  
825 into the land surface model JULES with an ensemble Kalman filter, *J Geophys Res-Atmos*, 115, 2010.  
826 Ghilain, N., Arboleda, A., Sepulcre-Canto, G., Batelaan, O., Ardo, J., and Gellens-Meulenberghs, F.:  
827 Improving evapotranspiration in a land surface model using biophysical variables derived from  
828 MSG/SEVIRI satellite, *Hydrology and Earth System Sciences*, 16, 2567-2583, 2012.  
829 Han, X., Li, X., Franssen, H. J. H., Vereecken, H., and Montzka, C.: Spatial horizontal correlation  
830 characteristics in the land data assimilation of soil moisture, *Hydrology and Earth System Sciences*, 16,  
831 1349-1363, 2012.  
832 Han, X. J., Franssen, H. J. H., Li, X., Zhang, Y. L., Montzka, C., and Vereecken, H.: Joint Assimilation of  
833 Surface Temperature and L-Band Microwave Brightness Temperature in Land Data Assimilation,  
834 *Vadose Zone J*, 12, 0, 2013.  
835 Han, X. J., Franssen, H. J. H., Montzka, C., and Vereecken, H.: Soil moisture and soil properties  
836 estimation in the Community Land Model with synthetic brightness temperature observations, *Water*  
837 *Resour Res*, 50, 6081-6105, 2014a.  
838 Han, X. J., Jin, R., Li, X., and Wang, S. G.: Soil Moisture Estimation Using Cosmic-Ray Soil Moisture  
839 Sensing at Heterogeneous Farmland, *IEEE Geoscience and Remote Sensing Letters*, 11, 1659-1663,  
840 2014b.  
841 Hunt, B. R., Kostelich, E. J., and Szunyogh, I.: Efficient data assimilation for spatiotemporal chaos: A  
842 local ensemble transform Kalman filter, *Physica D: Nonlinear Phenomena*, 230, 112-126, 2007.  
843 Jarlan, L., Balsamo, G., Lafont, S., Beljaars, A., Calvet, J. C., and Mougin, E.: Analysis of leaf area index  
844 in the ECMWF land surface model and impact on latent heat and carbon fluxes: Application to West  
845 Africa, *J Geophys Res-Atmos*, 113, 2008.  
846 Jin, R., Li, X., Yan, B., Li, X., Luo, W., Ma, M., Guo, J., Kang, J., Zhu, Z., and Zhao, S.: A Nested  
847 Ecohydrological Wireless Sensor Network for Capturing the Surface Heterogeneity in the Midstream  
848 Areas of the Heihe River Basin, China, *IEEE Geoscience and Remote Sensing Letters*, PP, 1-5, 2014.  
849 Jin, R., Wang, X., Kang, J., Wang, Z., Dong, C., and Li, D.: HiWATER: SoilNET observation dataset in the  
850 middle reaches of the Heihe river basin, Heihe Plan Science Data Center, doi:  
851 10.3972/hiwater.120.2013.db  
852 doi:10.3972/hiwater.120.2013.db, 2013. 2013.  
853 Kerr, Y. H., Waldteufel, P., Wigneron, J. P., Delwart, S., Cabot, F., Boutin, J., Escorihuela, M. J., Font, J.,  
854 Reul, N., Gruhier, C., and Others: The SMOS Mission: New Tool for Monitoring Key Elements of the  
855 Global Water Cycle, *P IEEE*, 98, 666--687, 2010.

856 Kumar, S. V., Reichle, R. H., Harrison, K. W., Peters-Lidard, C. D., Yatheendradas, S., and Santanello, J. A.:  
857 A comparison of methods for a priori bias correction in soil moisture data assimilation, *Water Resour*  
858 *Res*, 48, n/a-n/a, 2012.

859 Kumar, S. V., Reichle, R. H., Koster, R. D., Crow, W. T., and Peters-Lidard, C. D.: Role of Subsurface  
860 Physics in the Assimilation of Surface Soil Moisture Observations, *J Hydrometeorol*, 10, 1534-1547,  
861 2009.

862 Kustas, W. and Anderson, M.: Advances in thermal infrared remote sensing for land surface modeling,  
863 *Agr Forest Meteorol*, 149, 2071-2081, 2009.

864 Li, C. and Ren, L.: Estimation of Unsaturated Soil Hydraulic Parameters Using the Ensemble Kalman  
865 Filter, *Vadose Zone J*, 10, 1205, 2011.

866 Li, F. Q., Crow, W. T., and Kustas, W. P.: Towards the estimation root-zone soil moisture via the  
867 simultaneous assimilation of thermal and microwave soil moisture retrievals, *Adv Water Resour*, 33,  
868 201-214, 2010.

869 Li, X., Cheng, G. D., Liu, S. M., Xiao, Q., Ma, M. G., Jin, R., Che, T., Liu, Q. H., Wang, W. Z., Qi, Y., Wen, J.  
870 G., Li, H. Y., Zhu, G. F., Guo, J. W., Ran, Y. H., Wang, S. G., Zhu, Z. L., Zhou, J., Hu, X. L., and Xu, Z. W.:  
871 Heihe Watershed Allied Telemetry Experimental Research (HiWATER): Scientific Objectives and  
872 Experimental Design, *B Am Meteorol Soc*, 94, 1145-1160, 2013.

873 Miyoshi, T. and Yamane, S.: Local Ensemble Transform Kalman Filtering with an AGCM at a T159/L48  
874 Resolution, *Mon Weather Rev*, 135, 3841-3861, 2007.

875 Montzka, C., Grant, J. P., Moradkhani, H., Franssen, H. J. H., Weihermuller, L., Drusch, M., and  
876 Vereecken, H.: Estimation of Radiative Transfer Parameters from L-Band Passive Microwave Brightness  
877 Temperatures Using Advanced Data Assimilation, *Vadose Zone J*, 12, 2013.

878 Moradkhani, H., Sorooshian, S., Gupta, H. V., and Houser, P. R.: Dual state-parameter estimation of  
879 hydrological models using ensemble Kalman filter, *Adv Water Resour*, 28, 135-147, 2005.

880 Nie, S., Zhu, J., and Luo, Y.: Simultaneous estimation of land surface scheme states and parameters  
881 using the ensemble Kalman filter: identical twin experiments, *Hydrology and Earth System Sciences*,  
882 15, 2437-2457, 2011.

883 Oleson, K., Lawrence, D. M., Bonan, G., Drewniak, B., Huang, M., Koven, C. D., Levis, S., Li, F., Riley, W.  
884 J., Subin, Z. M., Swenson, S. C., Thornton, P. E., Bozbiyik, A., Fisher, B. E. A., Kluzek, E., Lamarque, J. F.,  
885 Lawrence, P. J., Leung, L. R., Lipscomb, W., Muszala, S., Ricciuto, D. M., Sacks, W., Sun, Y., Tang, J., and  
886 Yang, Z.-L.: Technical Description of version 4.5 of the Community Land Model (CLM), *Ncar Technical*  
887 *Note NCAR/TN-503+STR*, National Center for Atmospheric Research, Boulder, CO, 422 pp., 2013. 2013.

888 Pauwels, V. R. N., Balenzano, A., Satalino, G., Skriver, H., Verhoest, N. E. C., and Mattia, F.: Optimization  
889 of Soil Hydraulic Model Parameters Using Synthetic Aperture Radar Data: An Integrated  
890 Multidisciplinary Approach, *Ieee T Geosci Remote*, 47, 455-467, 2009.

891 Reichle, R. H.: Data assimilation methods in the Earth sciences, *Adv Water Resour*, 31, 1411-1418,  
892 2008.

893 Reichle, R. H., Kumar, S. V., Mahanama, S. P. P., Koster, R. D., and Liu, Q.: Assimilation of  
894 Satellite-Derived Skin Temperature Observations into Land Surface Models, *J Hydrometeorol*, 11,  
895 1103-1122, 2010.

896 Robinson, D. A., Jones, S. B., Wraith, J. M., Or, D., and Friedman, S. P.: A Review of Advances in  
897 Dielectric and Electrical Conductivity Measurement in Soils Using Time Domain Reflectometry, *Vadose*  
898 *Zone J*, 2, 444-475, 2003.

899 Rodell, M., Houser, P. R., Jambor, U., Gottschalck, J., Mitchell, K., Meng, C. J., Arsenault, K., Cosgrove,

900 B., Radakovich, J., Bosilovich, M., Entin, J. K., Walker, J. P., Lohmann, D., and Toll, D.: The global land  
901 data assimilation system, *B Am Meteorol Soc*, 85, 381-+, 2004.

902 Rosolem, R., Hoar, T., Arellano, A., Anderson, J. L., Shuttleworth, W. J., Zeng, X., and Franz, T. E.:  
903 Assimilation of near-surface cosmic-ray neutrons improves summertime soil moisture profile  
904 estimates at three distinct biomes in the USA, *Hydrol. Earth Syst. Sci. Discuss.*, 11, 5515-5558, 2014.

905 Rosolem, R., Shuttleworth, W. J., Zreda, M., Franz, T. E., Zeng, X., and Kurc, S. A.: The Effect of  
906 Atmospheric Water Vapor on Neutron Count in the Cosmic-Ray Soil Moisture Observing System, *J*  
907 *Hydrometeorol*, 14, 1659-1671, 2013.

908 Savitzky, A. and Golay, M. J. E.: Smoothing and Differentiation of Data by Simplified Least Squares  
909 Procedures, *Analytical Chemistry*, 36, 1627-1639, 1964.

910 Schwinger, J., Kollet, S. J., Hoppe, C. M., and Elbern, H.: Sensitivity of Latent Heat Fluxes to Initial  
911 Values and Parameters of a Land-Surface Model, *Vadose Zone J*, 9, 984-1001, 2010.

912 Shangguan, W., Dai, Y., Liu, B., Zhu, A., Duan, Q., Wu, L., Ji, D., Ye, A., Yuan, H., Zhang, Q., Chen, D.,  
913 Chen, M., Chu, J., Dou, Y., Guo, J., Li, H., Li, J., Liang, L., Liang, X., Liu, H., Liu, S., Miao, C., and Zhang, Y.:  
914 A China data set of soil properties for land surface modeling, *J Adv Model Earth Sy*, 5, 212-224, 2013.

915 Shuttleworth, J., Rosolem, R., Zreda, M., and Franz, T. E.: The COsmic-ray Soil Moisture Interaction  
916 Code (COSMIC) for use in data assimilation, *Hydrology and Earth System Sciences*, 17, 3205-3217,  
917 2013.

918 Sun, W. X., Liang, S. L., Xu, G., Fang, H. L., and Dickinson, R.: Mapping plant functional types from  
919 MODIS data using multisource evidential reasoning, *Remote Sens Environ*, 112, 1010-1024, 2008.

920 van den Hurk, B. J. J. M.: Impact of leaf area index seasonality on the annual land surface evaporation  
921 in a global circulation model, *Journal of Geophysical Research*, 108, 2003.

922 Wan, Z. and Li, Z. L.: Radiance - based validation of the V5 MODIS land - surface temperature product,  
923 *Int J Remote Sens*, 29, 5373-5395, 2008.

924 Xu, T. R., Liang, S. L., and Liu, S. M.: Estimating turbulent fluxes through assimilation of geostationary  
925 operational environmental satellites data using ensemble Kalman filter, *J Geophys Res-Atmos*, 116,  
926 D09109, doi: 10.1029/2010JD015150, 2011.

927 Xu, Z. W., Liu, S. M., Li, X., Shi, S. J., Wang, J. M., Zhu, Z. L., Xu, T. R., Wang, W. Z., and Ma, M. G.:  
928 Intercomparison of surface energy flux measurement systems used during the HiWATER-MUSOEXE, *J*  
929 *Geophys Res-Atmos*, 118, 13140-13157, 2013.

930 Yang, K., Koike, T., Kaihotsu, I., and Qin, J.: Validation of a Dual-Pass Microwave Land Data Assimilation  
931 System for Estimating Surface Soil Moisture in Semiarid Regions, *J Hydrometeorol*, 10, 780-793, 2009.

932 Yang, Z. L., Dai, Y., Dickinson, R. E., and Shuttleworth, W. J.: Sensitivity of ground heat flux to  
933 vegetation cover fraction and leaf area index, *J Geophys Res-Atmos*, 104, 19505-19514, 1999.

934 Zhu, C. Y., Byrd, R. H., Lu, P. H., and Nocedal, J.: Algorithm 778: L-BFGS-B: Fortran subroutines for  
935 large-scale bound-constrained optimization, *Acm Transactions on Mathematical Software*, 23, 550-560,  
936 1997.

937 Zreda, M., Desilets, D., Ferre, T. P. A., and Scott, R. L.: Measuring soil moisture content non-invasively  
938 at intermediate spatial scale using cosmic-ray neutrons, *Geophys Res Lett*, 35, L21402, 2008.

939 Zreda, M., Shuttleworth, W. J., Zeng, X., Zweck, C., Desilets, D., Franz, T. E., and Rosolem, R.: COSMOS:  
940 the COsmic-ray Soil Moisture Observing System, *Hydrology and Earth System Sciences*, 16, 4079-4099,  
941 2012.

942